Research Square

Preprints are preliminary reports that have not undergone peer review.
They should not be considered conclusive, used to inform clinical practice,
or referenced by the media as validated information.

Decadal Changes in the Low-Level Circulations over the Maritime Continent and Their Driving Mechanisms: Based on ERA5 Reanalysis

Alugula Boyaj

boyaj@nus.edu.sg

National University of Singapore https://orcid.org/0000-0002-9528-7475

Srivatsan Vijayaraghavan

National University of Singapore

Research Article

Keywords: Southeast Asia, Low-level monsoon circulation, Decadal variability, IOD, ENSO, Hydroclimate change, Maritime Continent

Posted Date: November 14th, 2026

DOI: https://doi.org/10.21203/rs.3.rs-11399327/v1

License: This work is licensed under a Creative Commons Attribution 4.0 International License.
Read Full License

Decadal Changes in the Low-Level Circulations over the Maritime Continent and Their Driving Mechanisms: Based on ERA5 Reanalysis

Alugula Boyaj, Srivatsan Vijayaraghavan*

Tropical Marine Science Institute, National University of Singapore, 119227, Singapore

**Corresponding author:*

Dr. Alugula Boyaj,
Research Fellow,
National University of Singapore (NUS),
Tropical Marine Science Institute (TMSI),
Climate and Weather Research Cluster,
18 Kent Ridge Rd, Singapore 119227.
boyaj@nus.edu.sg

Abstract

This study examines changes in 850-hPa circulation over Southeast Asia (SEA) using ERA5 reanalysis for 1985–2024. Two predefined 20-year periods (1985–2004 and 2005–2024) are compared to assess seasonal wind-speed (WS) differences, temporal trends, and associations with the El Niño–Southern Oscillation (ENSO) and Indian Ocean Dipole (IOD). During 2005–2024, easterlies intensified over oceanic regions in JJA and SON, while westerlies intensified over the Maritime Continent in DJF and MAM. Mean WS increased across much of the domain during JJA, DJF, and SON, although within-period trends were spatially heterogeneous, with negative trends more widespread during 2005–2024. Pettitt tests identified seasonally varying change points between 1993 and 2001, but only SON reached statistical significance, providing no evidence of a common abrupt transition. The percentile-based wind-year exclusion analysis indicates that the higher mean WS in the recent period is not solely driven by anomalously strong wind years, suggesting that moderate and lower wind regimes also contribute to the observed increase. ENSO-related WS associations were particularly evident during DJF, whereas IOD-related associations were more spatially extensive during JJA and SON, with increased coverage of significant IOD–WS partial correlations in the recent period. SST composites revealed pronounced zonal contrasts across the tropical Indian Ocean during IOD events, consistent with associated circulation anomalies. ERA5 precipitation analysis showed increased extreme rainfall intensity and frequency over parts of the equatorial Maritime Continent and the Philippines, alongside decreases over mainland SEA. These findings highlight spatially heterogeneous changes in regional circulation and hydroclimate, while their interpretation remains conditional on the predefined period division and ERA5 representation.

Keywords: Southeast Asia; Low-level monsoon circulation; Decadal variability; IOD; ENSO; Hydroclimate change; Maritime Continent

1. Introduction

Low-level atmospheric circulation at 850 hPa plays a fundamental role in shaping regional climate and weather systems, serving as a key indicator of monsoonal intensity, moisture transport, and large-scale circulation variability (Wang and Fan, 1999; Tangang et al., 2008; Purwar et al., 2023; Thapliyal, 2023). Given Southeast Asia's (SEA) complex land-sea interactions and pronounced monsoonal dynamics (Chang et al., 2005; Wang et al., 2012), understanding recent changes in 850 hPa circulation and their driving mechanisms is of considerable scientific and practical importance. SEA's climate is dominated by the Asian Australian monsoon system, which governs regional rainfall and low-level wind patterns (Wang, 2006; Qian et al., 2010). During summer (June–September), a strong south-westerly low-level jet develops over the South China Sea (SCS) and Bay of Bengal (BoB), whereas winter (December–February) is characterized by northeasterly winds driven by the Siberian High (Chan and Li, 2004; Xie et al., 2007; Ha et al., 2012). These monsoon circulations exhibit interannual to decadal variability, influenced by internal atmospheric processes and large-scale climate modes, particularly the El Niño–Southern Oscillation (ENSO) and Indian Ocean Dipole (IOD) (Aldrian and Susanto, 2003; Juneng and Tangang, 2005).

At the planetary scale, a growing body of literature has documented a weakening of the tropical overturning circulation under global warming, with broad implications for regional wind speed (WS), precipitation patterns, and moisture transport (Vecchi and Soden, 2007; Tokinaga et al., 2012; Chemke and Polvani, 2021). These large-scale changes, however, do not translate uniformly to the regional scale. Studies of the Asian monsoon region have linked changes in low-level monsoon circulation to land–sea thermal contrasts associated with differential warming (Kamae et al., 2014; Shaw and Voigt, 2015). Importantly, observed circulation changes over SEA may also reflect abrupt shifts rather than gradual monotonic trends, a distinction that has implications for how observed wind changes are interpreted and attributed (Li et al., 2023).

Superimposed on these large-scale dynamical changes are the regionally specific responses to Indo-Pacific SST variability. ENSO exerts a dominant influence on SSTs across the tropical Pacific and Indian Oceans, altering large-scale atmospheric circulation through teleconnection patterns that modulate WS and rainfall across SEA, with its suppressive influence over the Maritime Continent being particularly well documented (Klein et al., 1999; Juneng and Tangang, 2005). The IOD, characterized by anomalous SST gradients between the western and eastern tropical Indian Ocean (Saji et al., 1999), has emerged as a driver of regional climate variability, capable of reinforcing or partially offsetting ENSO-driven anomalies (Ashok et al., 2003; Cai et al., 2013). Recent evidence suggests that positive IOD events may increase under anthropogenic forcing, amplifying the zonal SST gradient and potentially strengthening monsoon inflow into the SEA circulation, which warrants closer examination.

The zonal and meridional components of the 850 hPa wind are integral to these interconnected processes. Changes in zonal wind modulate the position and intensity of the inter-tropical convergence zone (ITCZ) and the subtropical highs, while variations in meridional wind affect cross-equatorial flow and moisture transport into the continental interior (Wang et al., 2001; Geen et al., 2020; Kumari et al., 2025). Disentangling the contributions of these components across seasons and separating the roles of moderate versus extreme wind regimes is therefore essential for attributing observed circulation changes to specific dynamical mechanisms (Trenberth et al., 2000; Bansod et al., 2012).

Despite these advances, comprehensive analyses that simultaneously examine changes in zonal wind, meridional wind, and WS alongside their seasonal evolution, monsoonal changes, extreme wind contributions, and the distinct roles of ENSO and IOD remain limited for the SEA domain. For instance, Tangang et al. (2008) focused primarily on interannual wind variability driven by ENSO without addressing longer-term circulation shifts, while Kamae et al. (2014) examined monsoon intensification across Asia without resolving sub-regional heterogeneity within SEA. Similarly, studies of IOD impacts have largely focused on individual regions such as the

Maritime Continent or mainland SEA (Ashok et al., 2003; Du et al., 2009), leaving an integrated, domain-wide assessment across all seasons largely absent from the literature. The advent of high-resolution reanalysis products such as ERA5, with its improved representation of atmospheric dynamics at fine spatiotemporal scales, provides an opportunity to address these gaps (Hersbach et al., 2020; Tarek et al., 2020; Lavers et al., 2022; Xie et al., 2025).

Changes in low-level circulation over SEA are also closely coupled with regional hydroclimate variability. The monsoon-driven wind regimes govern moisture transport and convergence patterns that directly control the spatial distribution and intensity of rainfall across the region (Wang et al., 2001; Qian et al., 2010). Recent studies have documented contrasting rainfall trends across SEA, with increasing extreme precipitation over the equatorial Maritime Continent and the Philippines alongside drying tendencies over parts of mainland SEA, potentially linked to shifts in large-scale circulation and SST boundary conditions (Endo et al., 2009; Villafuerte and Matsumoto, 2015; Boyaj and Vijayaraghavan, 2025). Examining how circulation changes at 850 hPa are reflected in rainfall characteristics therefore provides an important observational constraint for understanding the broader hydroclimate implications of the circulation changes identified in this study.

This study therefore examines changes in 850-hPa circulation over SEA using ERA5 for 1985–2024, comparing two predefined 20-year periods (1985–2004 and 2005–2024). Specifically, we investigate (i) differences in zonal and meridional winds; (ii) annual and seasonal variations in WS and linear trends; (iii) the contributions of different WS categories and associations with ENSO and IOD; and (iv) accompanying changes in rainfall characteristics.

2. Datasets and Methodology

2.1 Datasets

This study uses the daily ERA5 reanalysis dataset from the European Centre for Medium-Range Weather Forecasts, providing gridded 850-hPa zonal and meridional wind components and

precipitation at ~25 km for 1985–2024 (Hersbach et al., 2020). ERA5 assimilates a wide range of in-situ and satellite observations through a four-dimensional variational scheme within the Integrated Forecasting System, offering improved physical parameterizations and high spatio-temporal resolution. These advancements make it one of the most reliable datasets for climate diagnostics, model validation, and decadal analyses. ERA5 has been widely adopted for atmospheric analyses, as illustrated by studies on tropical-cyclone prediction (Feng et al., 2022), rainfall extremes (Xu et al., 2022), topographic influences on low-level vortices (Ciesielski and Johnson, 2022), equatorial waves and heavy rainfall (Ferrett et al., 2023), vertical accuracy over complex terrain (Wei et al., 2024), regional climate model intercomparison (Hung et al., 2026), and global wind-wave hindcasting (Sharmar and Markina, 2020). ERA5 shows better agreement with observations for tropospheric temperature, wind, humidity, and wave height (Hersbach et al., 2020).

To examine the associated large-scale oceanic climate driver influences, we used the National Oceanic and Atmospheric Administration Optimum Interpolation Sea Surface Temperature (OISST) Version 2 dataset (Huang et al., 2021), which provides daily gridded SSTs at ~25 km resolution over the same period (1985–2024). OISST combines in situ and satellite observations with bias corrections and interpolation techniques to produce a temporally consistent record of global ocean surface temperatures. This dataset is widely used in studies of air–sea interactions, monsoon variability, and ocean–atmosphere coupling, providing an essential complement to wind-field analyses (Huang et al., 2013; Gupta and Sil, 2024; Swetha et al., 2025).

2.2 Methodology

The study covers 30°S–30°N and 80°E–150°E, encompassing mainland SEA, the Maritime Continent, and adjacent oceans. The 1985–2024 record was divided into two non-overlapping, equal-length intervals, 1985–2004 and 2005–2024, to compare past and recent climatological conditions using equivalent sample durations. Previous studies describe substantial Indo-Pacific

variability around the late 1990s and early 2000s, including changes related to the Interdecadal Pacific Oscillation (Kosaka and Xie, 2013; Meehl et al., 2014; Trenberth et al., 2014). This context motivates examining differences across the broader interval, but does not establish 2005 as a unique, statistically detected transition year. Accordingly, the two intervals are treated as fixed comparison windows, not as independently verified climate regimes. The sensitivity of results to other dividing years was not evaluated and remains a limitation.

WS at 850 hPa was calculated as the magnitude of the zonal (U) and meridional (V) components. Seasonal means were obtained for December–February (DJF), March–May (MAM), June–August (JJA), and September–November (SON). Anomalies were referenced to the 1985–2024 climatology, and area-averaged series were used to examine interannual variability. Ordinary least-squares linear trends in WS were estimated at each grid point for 1985–2024 and separately for the fixed periods 1985–2004 and 2005–2024 (m s^{-1} $decade^{-1}$). The manuscript reports two-tailed Student's t-tests at $p < 0.05$ (Wilks, 2011). These tests do not explicitly account for temporal autocorrelation or spatial multiplicity, which should be considered when interpreting the extent of statistical significance.

As an exploratory diagnostic, the nonparametric Pettitt test (Pettitt, 1979) was applied independently to the complete 1985–2024 area-averaged seasonal WS anomaly series, without imposing the 2005 boundary. The test identifies an estimated change point in the location parameter of each time series, commonly interpreted as a shift in its median (Villarini et al., 2009; Liu et al., 2012; Mallakpour and Villarini, 2016). Because serial dependence can affect nominal significance, and no autocorrelation-adjusted resampling was undertaken, nonsignificant change points are discussed only as exploratory features. The Pettitt results were not used to select the fixed 20-year comparison windows.

The contribution of wind regimes to seasonal mean WS was examined using two complementary approaches. First, years in which seasonal mean WS anomalies exceeded one standard deviation above the long-term mean were identified to isolate anomalously strong wind years. Second,

percentile-based thresholds, the 25th, 50th, 75th, and 95th percentiles, were applied to classify WS into low, moderate, high, and extreme regimes, respectively. Climatological differences between the two sub-periods were then recomputed after cumulatively excluding from the recent period only, the years at or above the 95th, 75th, 50th, and 25th percentile thresholds. These exclusion experiments are exploratory sensitivity tests of how strongly the period means depend on different parts of the WS distribution.

To identify dominant spatial modes of WS variability, Empirical Orthogonal Function (EOF) analysis was applied to monthly WS anomalies separately for each climate period (Björnsson and Venegas, 1997; Wilks, 2011). EOF patterns were expressed as correlations between the principal component time series and the anomaly field at each grid point. The leading modes (EOF1 and EOF2) were interpreted as representing large-scale monsoonal circulation variability and regional land–sea contrasts, respectively, and explained variance was compared between periods to assess changes in dynamical coherence.

The influence of large-scale climate drivers was examined through partial correlation and composite analyses. The Niño3 index (5°N–5°S, 150°W–90°W) was used to characterize ENSO variability, capturing the canonical ENSO signal most relevant to Indo-Pacific teleconnections (Rasmusson and Carpenter, 1982). The IOD index was defined as the SST anomaly difference between the western (50°E–70°E, 10°S–10°N) and eastern (90°E–110°E, 10°S–0°N) equatorial Indian Ocean (Saji et al., 1999). Partial correlations isolated the association of each mode with seasonal WS anomalies, and composites of strong positive and negative events were constructed to examine associated wind and SST anomaly patterns.

To assess the hydrological response to circulation changes, seasonal rainfall characteristics were analyzed using differences in seasonal mean rainfall, percentile-based intensities (25th, 50th, 75th, and 95th percentiles), and rainfall frequency distributions across daily thresholds of 1, 5, 10, 15, and 20 mm/day, following the Expert Team on Climate Change Detection and Indices (ETCCDI) framework for precipitation extremes (Zhang et al., 2011). This enabled a

comprehensive characterization of both the magnitude and frequency of rainfall changes associated with evolving monsoon winds and large-scale climate forcing over SEA.

3. Results and Discussion

3.1 Changes in Zonal and Meridional Wind Components

We first examined changes in the U and V wind components at 850 hPa to identify variations in wind direction and magnitude between the past and recent climate periods. These circulation changes are crucial for understanding shifts in cross-equatorial flow and moisture transport that influence rainfall patterns over SEA. To assess these variations, we analyzed spatial patterns to highlight land–ocean contrasts and localized intensification or weakening of winds. Additionally, longitudinal means of the zonal wind and latitudinal means of the meridional wind were computed to summarize broader regional circulation features.

3.1.1 Zonal wind

The spatial distribution of the climatological zonal wind and its changes between the recent and past climate periods for the four seasons over SEA are shown in Figure 1. Tropical easterlies (westward flow) dominate the belt from 30°S to 10°S throughout the year, with magnitudes of 1.7–6 m s^{-1}, weakest in DJF and strongest in JJA when their north–south extent broadens. Additional easterly cores occur between 10°N and 20°N, most intense in DJF (~6 m s^{-1}) and persisting through the other seasons with slight eastward extensions (110°–150°E in MAM/SON, 130°–150°E in JJA). Subtropical and equatorial westerlies (eastward flow) are most pronounced between 20°N and 30°N in DJF and MAM, and along 5°S–5°N during DJF, MAM, and SON, exceeding 6 m s^{-1} in DJF. The strongest westerlies occur in JJA (up to >6 m s^{-1} over 0°–25°N, 80°–130°E), representing the core of the summer monsoonal flow (Figure 1, first and second columns).

Differences between the two climate periods (Figure 1, third column) reveal that changes are both seasonally and regionally dependent. Intensification of easterlies (~0.3–1 m s^{-1}, $p < 0.05$)

occurs over 10°N–20°N and 30°S–20°S in DJF and MAM, and over 30°S–20°N in JJA and SON, primarily across oceanic regions. Conversely, westerlies have intensified over the Maritime Continent (10°S–10°N), with peak intensification of ~1 m s^{-1} in DJF and MAM and weaker, more localized increases in JJA and SON. These areas of intensified westerlies may be associated with changes in low-level moisture transport toward the equatorial zone, although moisture transport was not diagnosed here. The longitudinal averages of zonal wind differences between the two climate periods (Figure 2, top row) support these findings, showing consistent intensification of easterlies over the 30°S–20°S and 10°N–30°N latitude bands in DJF and MAM (Figure 2a and b), and over 30°S–10°N in JJA and SON (Figure 2c and d). Intensification of westerlies is mainly confined to the 20°S–10°N latitude band during DJF and MAM (Figure 2a and b), consistent with stronger westerly flow over the equatorial Maritime Continent.

3.1.2 Meridional wind

The spatial distribution of the climatological meridional wind and its differences between the two climate periods are shown in Figure S1. During DJF, northerlies (southward flow) dominate 0–30°N, while southerlies (northward flow) prevail over the eastern Indian Ocean, reflecting the winter monsoon circulation. As the transition toward the summer monsoon begins in MAM, southerlies extend northward across 10°N–30°N and the Indian Ocean, while northerlies persist over the western Pacific. The mature summer monsoon in JJA is characterized by strong southerly flows across most of SEA, except over western Australia. By SON, southerlies remain dominant over the Indian Ocean, whereas northerlies re-emerge over the South China Sea and western Pacific (Figure S1, first and second columns).

Differences between the two periods (Figure S1, third column) highlight regionally enhanced meridional flows, with intensified northerlies (~0.3–0.8 m s^{-1}, significant locally at $p < 0.05$) over parts of mainland SEA and adjacent land areas during DJF, MAM, and JJA, most clearly in MAM, and intensified southerlies (~0.2–0.6 m s^{-1}) over oceanic regions during MAM, JJA, and SON. The latitudinal averages (Figure 2, bottom row) further illustrate broad intensification

of northerlies around 90°E and 100°E–118°E in DJF (Figure 2e), 100°E–140°E in MAM (Figure 2f), and 100°E–120°E in JJA (Figure 2g), while southerly intensification is evident over 120°E–140°E in DJF and JJA, and 80°E–150°E in SON (Figure 2h).

Taken together, the U and V fields indicate seasonally and regionally varying changes, including stronger easterly components over parts of the surrounding oceans during JJA and SON and stronger westerly components in parts of the Maritime Continent during DJF and MAM. These circulation differences may influence moisture transport and convergence, but the wind-component diagnostics alone do not quantify moisture-flux convergence or establish a rainfall response.

3.2 Spatio-temporal Variability of Wind Speed

After examining the U and V components separately, we next focus on the 850 hPa WS, which represents the combined strength of the low-level flow. WS is a key indicator of monsoon intensity and lower-tropospheric circulation strength, directly influencing moisture transport and rainfall variability over SEA (Chang et al., 2005).

3.2.1 Annual cycle

Figure S2 compares the annual cycle of area-averaged 850-hPa WS for 1985–2004 and 2005–2024. Both periods show higher WS around January–February and June–August and lower WS around April and October–November. The recent-minus-past difference is positive in January, May–July, September, and October–December, but negative in February–April and August. These month-to-month contrasts indicate that the inter-period difference is not a uniform increase throughout the year.

3.2.2 Spatial changes in seasonal wind speed

Figure 3 illustrates the spatial distribution of the seasonal climatological WS and wind vectors for both climate periods, while Figure 4 presents the corresponding longitudinal and latitudinal WS differences across the four seasons. Because the spatial climatology of WS largely mirrors

277 that of the zonal wind component (Figure 1), the discussion focuses on inter-period changes and
278 their regional significance.

279 The difference fields (Figure 3, third column) reveal statistically significant ($p < 0.05$) seasonal
280 and regional variations in WS across SEA. During DJF (Figure 3c), WS intensifies by
281 approximately 0.5–1 m s^{-1} over the eastern Philippines, the southern equatorial Indo-Pacific (0°–
282 10°S), the northern BoB, and the SCS, indicating an intensified northeasterly monsoon flow.
283 Negative anomalies of comparable magnitude over 0°–10°N may reflect weakened local
284 convergence or a southward displacement of the low-level convergence zone. The longitudinal
285 and latitudinal means (Figures 4a, 4e) confirm broad WS intensification across 10°N–20°N,
286 30°S–20°S, and 10°S–0°, with modest reductions (~0.3 m s^{-1}) near the equator and 20°N.

287 In MAM (Figure 3f), positive WS differences of 0.2–0.4 m s^{-1} occur over the Bay of Bengal and
288 eastern equatorial Indian Ocean, whereas decreases of 0.2–0.3 m s^{-1} occur over northwestern
289 mainland SEA, the South China Sea, and parts of the southern equatorial Indo-Pacific. The zonal
290 and meridional averages (Figures 4b and 4f) indicate higher WS west of approximately 105°E
291 and lower WS farther east. These patterns describe a spatial contrast in the period means; an
292 earlier monsoon onset or a change in land–sea thermal contrast cannot be established from these
293 maps alone.

294 During JJA (Figure 3i), the most pronounced intensification occurs, with WS increases of up to
295 0.8 m s^{-1} over the southeastern Indian Ocean, western Pacific, and eastern SCS, reflecting an
296 intensified southwest monsoon. Concurrent decreases of 0.2–0.3 m s^{-1} over the northern BoB
297 suggest weakened local convergence. The averaged profiles (Figures 4c, 4g) highlight WS
298 intensification between 20°S and the equator and east of 100°E, indicating a latitudinal
299 redistribution of monsoonal momentum.

In SON (Figure 3l), WS intensifies by 0.4–0.6 m s^{-1} over the southern equatorial Indo-Pacific, BoB, and East China Sea, reflecting stronger post-monsoon easterlies and residual cross-equatorial flow. Minor reductions below 0.2 m s^{-1} near the equator and around 20°N suggest localized adjustments within the retreating monsoon circulation. The domain-averaged profiles (Figures 4d, 4h) show a net WS increase across 80°E–150°E, consistent with intensified low-level circulation during the post-monsoon transition.

The domain-wide fractional analysis reveals seasonal differences in WS changes, with positive (negative) differences covering approximately ~64% (36%) of grid cells in DJF, ~43% (57%) in MAM, ~71% (29%) in JJA, and ~61% (39%) in SON. Thus, WS intensification predominated during JJA, DJF, and SON in 2005–2024 relative to 1985–2004, whereas weakening was more widespread during MAM. These findings highlight seasonal and spatial variability in WS changes, representing differences between the climatological means of two predefined periods rather than evidence of an abrupt circulation regime shift.

3.2.3 Temporal changes in seasonal wind speed

Figure 5 illustrates the spatial distribution of temporal trends in seasonal WS across three periods: 1985–2024, 1985–2004, and 2005–2024. During the long-term period (1985–2024), spatial and seasonal variations are pronounced, with positive trends generally concentrated over the southern tropics and marginal seas, while negative trends prevail over parts of the northern equatorial belt. In DJF, significant positive trends (0.4–0.6 m s^{-1} $decade^{-1}$) occur over the northern tropics (10°N–20°N) and the southern equatorial belt (10°S–0°), while comparable negative trends dominate the northern equatorial region (0°–10°N, 80°E–150°E). In MAM, positive trends (0.2–0.4 m s^{-1} $decade^{-1}$) are concentrated over the BoB and southeastern Indian Ocean, with negative trends of similar magnitude over northern SEA (20°N–30°N) and southern tropical latitudes (20°S–10°S). During JJA, widespread positive trends (0.2–0.5 m s^{-1} $decade^{-1}$) over the SCS, western equatorial Pacific, and southeastern Indian Ocean suggest intensified

summer monsoon winds. In SON, positive trends (0.2–0.4 m s^{-1} $decade^{-1}$) emerge over the southeastern Indian Ocean, the southwestern Pacific, and BoB, while negative trends appear across parts of the central western Pacific.

Trends also differ between the two fixed sub-periods. During 1985–2004, positive WS trends occur over extensive parts of the Indian Ocean and Maritime Continent, reaching approximately 0.7 m s^{-1} $decade^{-1}$ in some areas (Figure 5, second column). During 2005–2024, negative trends are more widespread in several seasons, with local values of approximately −0.2 to −0.8 m s^{-1} $decade^{-1}$ (Figure 5, third column). Figure S3 shows increasing area-averaged WS during 1985–2004 in DJF, JJA and SON (nearly flat in MAM) and decreasing tendencies during 2005–2024 in MAM, JJA and SON (nearly flat in DJF). These trends are conditional on the selected intervals and should not be interpreted as independently detected regime boundaries. Trends over 20-year windows are also strongly influenced by internal variability (Hawkins and Sutton, 2009; Deser et al., 2012), and few of the sub-period trends are statistically significant (hatching in Figure 5).

The proportion of grid cells with positive WS trends was lower in 2005–2024 than in 1985–2004: 57.92% versus 41.28% in DJF, 58.71% versus 44.36% in MAM, 69.50% versus 47.68% in JJA, and 56.13% versus 43.77% in SON. The largest decrease in this fraction (21.82 percentage points) occurred in JJA. These percentages describe the sign of the fitted trends, not the proportion of statistically significant trends. Comparisons with prior work on monsoon changes (Song et al., 2014; Kitoh, 2017; Kajikawa et al., 2010) provide context but do not identify the causes of the ERA5 trends reported here.

Thus, higher seasonal mean WS in parts of the domain during 2005–2024 can coexist with negative trends within-period. The combination indicates nonuniform temporal evolution but does not establish an abrupt increase in the mean circulation state. Section 3.3.1 explores potential seasonal change points independently using the full 1985–2024 series.

3.3 Factors Associated with Inter-Period Wind-Speed Differences

The fixed-period comparisons show higher seasonal mean WS over substantial portions of SEA during 2005–2024, whereas trends within that period are often negative. To characterize these differences, we examine (i) possible abrupt changes in seasonal WS using the Pettitt test and (ii) the contribution of various percentiles of WS categories. These diagnostics are complementary; they do not, individually or together, constitute a formal attribution of the period-mean changes.

3.3.1 Exploratory Pettitt Test

The Pettitt test was applied to the complete 1985–2024 area-averaged seasonal WS anomaly series (Figure 6), independently of the predefined 2005 comparison boundary. The estimated change points occur in 1996 (DJF), 1997 (MAM), 1993 (JJA), and 2001 (SON), with only SON reaching the nominal 95% significance level. Thus, the analysis does not identify a common statistically significant transition across seasons, as the estimated change points in DJF, MAM, and JJA are not statistically significant.

The seasonal series exhibit different patterns around their estimated change points (Figure 6). In DJF, JJA, and SON, the mean anomalies are higher after the estimated change points than before them. In MAM, the post-change-point mean anomaly is only slightly higher, followed by a declining tendency, indicating no clear abrupt shift, consistent with the non-significant Pettitt result. SON exhibits the most pronounced difference around 2001, consistent with its statistically significant change point. Following the estimated change points, DJF remains approximately stable, whereas MAM, JJA, and SON exhibit slight declining tendencies. However, these patterns should be interpreted cautiously, particularly for seasons without statistically significant change points.

The SON result provides evidence of a change in the location of its area-averaged seasonal WS series around 2001, subject to the assumptions of the standard Pettitt test. For DJF, MAM, and JJA, the estimated change points are descriptive and do not establish regime shifts. These tests

cannot demonstrate that the higher 2005–2024 mean WS in some regions arose from a single abrupt upward step. The observed inter-period differences may reflect a combination of interannual to decadal internal variability (Deser et al., 2010), nonlinear evolution, and changes in the distribution of stronger and weaker WS years.

3.3.2 Contribution of different wind speed categories

We assessed whether a small number of anomalously strong WS years account for the higher mean WS in parts of the recent period. For each season, years with area-averaged seasonal WS anomalies greater than one standard deviation above the 1985–2024 mean were classified as anomalously strong years. Over the full record these were: DJF: 2001, 2006, 2008, 2017, 2021, 2023; MAM: 2000, 2008, 2012, 2024; JJA: 2002, 2004, 2006, 2013, 2018, 2019; SON: 2006, 2008, 2009, 2013, 2024. Only those falling within 2005–2024 (DJF: 2006, 2008, 2017, 2021, 2023; MAM: 2008, 2012, 2024; JJA: 2006, 2013, 2018, 2019; SON: 2006, 2008, 2009, 2013, 2024) were excluded from the recent period, and the climatological difference maps were recomputed and compared with the original maps (Figure S4).

Removing anomalously strong years changes the magnitude of some local WS differences but leaves much of the broad spatial pattern visible (Figure S4; second column). This suggests that the inter-period mean differences are not solely attributable to a few anomalously strong seasons. Because exclusion also changes the sample size and composition, the maps should not be interpreted as a formal causal decomposition.

To further isolate the contributions of the mean differences to different wind regime classes, a percentile-based analysis was conducted using the 95th, 75th, 50th, and 25th percentiles of area-averaged seasonal WS over 1985–2024 were used as thresholds to represent extreme, high, moderate, and low WS conditions, respectively. For each season, the WS values corresponding to these percentiles were derived from the area-averaged WS time series for 1985–2024, and years falling within each category were subsequently identified. To assess each regime's

399 contribution to recent changes, the years corresponding to each percentile category were
400 systematically excluded from the recent climate period, and the climatological differences
401 between the recent and past periods were recalculated (Figure 7). Because the exclusion is
402 applied only to the recent period, removing progressively larger fractions of its higher-WS years
403 necessarily lowers its mean; the progressive weakening and eventual reversal of the differences
404 in Figure 7 are therefore expected by construction and do not by themselves quantify the
405 contribution of individual percentile classes.

406 The contributions of different WS percentile classes vary both seasonally and regionally (Figure
407 7). During DJF, the full-period differences indicate that the southeastern Indian Ocean
408 experienced a significant increase of approximately 0.8 m s^{-1} at the 95% confidence level (Figure
409 7, first row). Excluding 95th-percentile years reduces the mean bias to 0.5 m s^{-1}; further
410 excluding 75th-percentile years reduces it to 0.3 m s^{-1}; and excluding 50th-percentile years yields
411 a negative bias of −0.2 m s^{-1}. These results indicate that moderate-wind years (50th percentile)
412 exert a relatively larger influence on the observed intensification than extreme events alone. A
413 similar pattern is evident over the 10°S–0° region and the Philippine Sea, where significant WS
414 increases of approximately 1 m s^{-1} are observed. Over the Philippine Sea, excluding 25th-
415 percentile years produces a negative bias of approximately −0.5 m s^{-1}, highlighting the dominant
416 role of moderate and lower wind events in driving mean WS intensification in this region. During
417 MAM (Figure 7, second row), WS intensification over the BoB is primarily driven by 95th- and
418 75th-percentile years. During JJA (Figure 7, third row), moderate to lower percentiles (75th,
419 50th, and 25th) play a more significant role, while during SON (Figure 7, fourth row), 75th- and
420 50th-percentile years contribute most substantially.

421 Overall, the exclusion experiments indicate that the higher mean WS observed across several
422 regions during 2005–2024 cannot be attributed solely by anomalously strong wind years (≥95th
423 percentile). Although excluding years associated with lower percentile thresholds produces

larger changes produced by removing the ≥75th-, ≥50th-, and ≥25th-percentile years mainly reflects the reduction and composition of the recent-period sample. Therefore, the results suggest that the observed WS intensification is not driven exclusively by extreme events, but do not establish the independent contributions of moderate and low wind regimes (≥75th-, ≥50th-, and ≥25th) or provide conclusive evidence of an abrupt shift in the background circulation.

3.4 Associations with Large-Scale Climate Modes: ENSO and IOD

Given the established influence of Indo-Pacific Ocean–atmosphere variability on regional monsoon circulation, we next examine the associations of WS anomalies with two major climate modes, ENSO and IOD.

To characterize the dominant spatial patterns of WS variability, EOF analysis was performed on monthly WS anomalies separately for 1985–2004 and 2005–2024 (Figure S5). EOF1 (Figure S5, top row) exhibits a spatial pattern characterized by anomalies of one sign over the BoB, Indochina, and approximately 5°S–15°S, with opposite-signed anomalies over the western North Pacific, near-equatorial regions, and subtropical southern Indian Ocean. This pattern broadly resembles the spatial organization of regional monsoon and trade-wind variability. EOF1 explains approximately 26.7% of the total variance during 1985–2004 and 29.4% during 2005–2024. EOF2 (Figure S5, bottom row) captures contrasting anomalies between the South China Sea, Indochina, and Borneo and the subtropical southern Indian Ocean and northern Australia, accounting for approximately 13–14% of the variance in both periods. Although the explained variance of EOF1 increases slightly in the recent period, the difference is less than three percentage points and should not be interpreted as evidence of a substantial change in large-scale circulation influence without accounting for sampling uncertainty (North et al., 1982). Therefore, the associations between WS variability and ENSO and IOD are examined directly using partial correlation and composite analyses.

ENSO-related associations: Partial correlation analysis between the Niño3 index and seasonal WS anomalies (Figure S6) reveals pronounced spatial and seasonal differences. Negative correlations occur over parts of the equatorial Maritime Continent, particularly during DJF, suggesting that El Niño conditions are associated with reduced WS in these regions. However, positive correlations are also evident elsewhere, indicating that ENSO-related wind responses are spatially heterogeneous. Composite differences between El Niño and neutral years and between La Niña and neutral years (Figure S7) further demonstrate contrasting regional WS anomalies across seasons. These patterns are consistent with the influence of ENSO-related changes in tropical Pacific convection and Walker circulation on regional low-level winds (Klein et al., 1999; Juneng and Tangang, 2005). Nevertheless, the observed correlations and composites do not establish a uniform suppressive influence of ENSO across SEA or demonstrate a statistically significant change in ENSO influence between the two periods.

IOD-related associations: The partial correlations between the IOD index and seasonal WS anomalies (Figure 9) also exhibit considerable spatial and seasonal variability, with relatively extensive statistically significant associations during JJA and SON. Composite analysis of positive IOD (PIOD) and negative IOD (NIOD) events relative to neutral conditions, together with their differences (Figure 8), reveals contrasting WS anomalies over the equatorial Indian Ocean and Maritime Continent. The direction and magnitude of these anomalies vary geographically, indicating that positive IOD conditions are not uniformly associated with increased WS throughout the study domain. Nevertheless, the spatial patterns suggest that IOD variability is an important large-scale correlate of seasonal WS, particularly during JJA and SON.

The physical relationship between IOD variability and regional circulation is associated with changes in zonal SST gradients across the tropical Indian Ocean. During PIOD events, relatively warmer SSTs in the western Indian Ocean and cooler SSTs in the eastern basin modify atmospheric convection and pressure gradients, generating anomalous low-level winds that

influence circulation over the equatorial Indian Ocean and Maritime Continent (Saji et al., 1999; Webster et al., 1999; Ashok et al., 2003). Previous studies have also suggested that greenhouse warming may influence the frequency and intensity of certain classes of PIOD events (Cai et al., 2013; Cai et al., 2021). However, the present analysis does not independently quantify anthropogenic contributions to IOD variability or establish whether changes in IOD activity are responsible for the observed inter-period mean WS differences.

The spatial extent of statistically significant positive IOD–WS partial correlations increases from 14.50% during 1985–2004 to 19.46% during 2005–2024 in JJA and from 5.04% to 11.38% in SON (Figure 9). These increases indicate that positive IOD–WS associations occupy a larger fraction of the study domain in the recent period, particularly during the seasons when IOD variability is most prominent. However, differences in the spatial coverage of statistically significant correlations do not necessarily indicate statistically significant changes in correlation strength or establish a causal increase in IOD influence.

To further examine the oceanic conditions associated with IOD variability, composite SST differences between PIOD and NIOD events were analyzed for both climate periods (Figure 10). The composites exhibit pronounced zonal SST contrasts across the tropical Indian Ocean, particularly during JJA and SON, with relatively warmer conditions in the western basin and cooler conditions toward the eastern Indian Ocean and Maritime Continent. The spatial distribution and magnitude of these contrasts differ between the two periods, with the recent-period composites showing pronounced cooling over parts of the eastern Indian Ocean and Maritime Continent. These patterns are consistent with the characteristic SST structure of IOD variability and provide a physically plausible context for the associated regional wind anomalies. However, the composite differences do not independently demonstrate that changes in IOD forcing caused the observed increases in seasonal mean WS.

Overall, the partial correlation and composite analyses indicate that both ENSO and IOD are associated with seasonal WS variability over SEA, with particularly extensive IOD-related associations during JJA and SON. The accompanying SST contrasts provide a physically consistent explanation for the spatially heterogeneous wind anomalies associated with IOD events. Nevertheless, these statistical relationships should be distinguished from formal attribution of the inter-period mean WS differences, which may also reflect other modes of internal climate variability and external forcing. Together, the results highlight the importance of Indo-Pacific Ocean–atmosphere variability in modulating regional low-level circulation without establishing a single dominant cause of the observed decadal differences.

3.5 Changes in Rainfall Characteristics Between Two Climate Periods

To further assess rainfall changes accompanying the circulation differences, rainfall characteristics were analyzed between the past and recent climate periods using ERA5 reanalysis data. The analysis encompasses differences in seasonal mean rainfall, percentile-based rainfall intensities (25th, 50th, 75th, and 95th percentiles), and rainfall frequency distributions for thresholds of 1, 5, 10, 15, and 20 mm/day. ERA5 precipitation has been evaluated against observations at global and regional scales (Lavers et al., 2022; Tarek et al., 2020), but it is a model-derived product, and its fidelity over SEA may differ from station-based or satellite datasets, particularly over complex terrain and small island regions. A systematic validation against independent observational datasets is recommended as a subject for future work.

Several mechanisms could link the observed wind and rainfall patterns. Changes in low-level flow can modify moisture transport and convergence, while SST-related circulation anomalies can influence convection across the Maritime Continent and adjacent oceans (Wang et al., 2001; Trenberth et al., 2000). However, this study does not calculate vertically integrated moisture transport or moisture-flux convergence, and co-located wind and rainfall differences alone cannot establish a causal linkage. We therefore interpret the rainfall diagnostics as accompanying hydroclimatic changes rather than as an independently verified response to the WS differences.

The spatial patterns of seasonal mean rainfall differences (mm/day) between the recent and past climate periods (Figure S8, third column) reveal distinct regional and seasonal variations across SEA. The recent period exhibits a general increase in rainfall over equatorial regions, most evident in DJF, JJA, and SON. Statistically significant (95% confidence level) increases of 2–3 mm/day or more are observed over the Maritime Continent, the Philippines, and surrounding oceanic regions. In contrast, rainfall decreases over parts of northern and western mainland SEA, particularly in MAM, JJA and SON, indicating spatially heterogeneous changes across seasons.

The rainfall-percentile differences in Figure 11 (P95, P75, P50, and P25) vary considerably across seasons and regions. Positive P95 differences occur over several equatorial maritime areas, while negative anomalies appear over other sectors, including portions of mainland SEA. The lower percentiles exhibit more mixed spatial patterns. Figure 12 presents differences in the frequency of days exceeding specified rainfall thresholds, a diagnostic distinct from the percentile map. Together, these figures indicate heterogeneous changes in ERA5 rainfall intensity and occurrence rather than uniform intensification across Southeast Asia.

Rainfall-frequency differences (Figure 12) broadly resemble several intensity patterns. The frequency of heavier rainfall above selected thresholds increases in parts of the Maritime Continent and the Philippines, while decreases occur in portions of mainland SEA. Changes at lower thresholds are spatially mixed. Although some regions with higher WS also show more frequent heavy rainfall, their spatial correspondence does not establish that IOD-related circulation changes caused the precipitation differences.

Overall, the ERA5 diagnostics show spatially contrasting changes in rainfall intensity and frequency between the two fixed periods: increases in several metrics across equatorial maritime areas and decreases in parts of mainland SEA. These patterns may be dynamically connected to circulation variability, but their mechanisms require targeted moisture-budget analysis and validation with independent rainfall observations. These findings remain conditional on the predefined 2005 boundary; alternative split-year sensitivity tests, autocorrelation-aware change-

point significance, independent precipitation validation, and moisture-flux diagnostics would be valuable future extensions.

4. Summary and Conclusions

This study analyzed ERA5 850-hPa winds and associated rainfall characteristics over SEA and adjacent oceans during 1985–2024. We compared two predefined equal-length intervals, 1985–2004 and 2005–2024, and assessed full-record and within-period WS trends, exploratory seasonal change points, percentile-based exclusion experiments, and associations with ENSO and IOD. The fixed comparison windows describe past and recent conditions; they are not intended to identify a unique regime boundary in 2005.

During the recent period, easterly winds intensified considerably over oceanic regions, particularly during JJA and SON, while westerlies intensified across the Maritime Continent during DJF and MAM. WS analysis corroborates this pattern, showing an overall intensification in the recent period, most notably during JJA, DJF, and SON, when positive WS anomalies covered approximately 60–70% of the domain. Intensified WS over the SCS, BoB, and equatorial Indo-Pacific reflects stronger monsoon flow.

The trends provide a different perspective from the mean differences. Positive WS trends are more widespread during 1985–2004, whereas negative trends occur over larger areas during 2005–2024. These patterns do not contradict higher recent-period mean WS in several regions, because period means and within-period slopes measure different properties. The Pettitt test estimates seasonal change points between 1993 and 2001, but only SON is statistically significant at the nominal 95% level. Thus, the evidence does not support a common abrupt regime shift across seasons. Excluding anomalously strong years leaves much of the spatial pattern of period-mean differences intact, suggesting that the contrast is not restricted to a few strong-wind seasons.

The circulation patterns also vary with large-scale ocean–atmosphere variability. Partial correlations and composites show ENSO-related WS anomalies and substantial IOD–WS associations, especially in JJA and SON. The fraction of grid cells with significant positive IOD–WS correlations increases from 14.50% to 19.46% in JJA and from 5.04% to 11.38% in SON between the two periods. These findings support an association with Indian Ocean SST variability, but neither the correlation differences nor the composites demonstrate that IOD changes were the primary cause of the period-mean WS contrasts or establish an anthropogenic contribution.

ERA5 rainfall diagnostics show increases in several heavy-rainfall metrics over parts of the equatorial Maritime Continent and the Philippines, alongside decreases over portions of mainland SEA. These patterns are broadly consistent with spatially heterogeneous circulation changes, although moisture-budget diagnostics and independent precipitation validation are needed to assess the mechanisms and uncertainty.

In summary, the analysis documents substantial seasonal and regional differences in low-level circulation and rainfall between the past and recent portions of the ERA5 record. Interpretation is limited by the predefined 2005 boundary, the lack of dividing-year sensitivity tests, possible temporal dependence in significance testing, and the observational nature of the ENSO/IOD and rainfall analyses. Future work should test alternative period boundaries, evaluate change-point significance under autocorrelation, and use moisture-budget and attribution methods to clarify the drivers of the reported changes.

Funding Statement: No funding available.

Conflict of Interest: The authors declare no competing interests.

Ethics Approval: Not applicable.

Consent to Participate: Not applicable.

Consent for Publication: All authors consent to publish all details in the manuscript.

Data and Code Availability: Accessible upon request.

References

Aldrian, E. and Susanto, R., 2003. Identification of three dominant rainfall regions within Indonesia and their relationship to sea surface temperature. International Journal of Climatology, 23(12), pp.1435-1452.

Ashok, K., Guan, Z. and Yamagata, T., 2003. Influence of the Indian Ocean Dipole on the Australian winter rainfall. Geophysical Research Letters, 30(15).

Bansod, S.D., Singh, H.N., Patil, S.D. and Singh, N., 2012. Recent changes in the circulation parameters and their association with Indian summer monsoon rainfall. Journal of Atmospheric and Solar-Terrestrial Physics, 77, pp.248-253.

Björnsson, H. and Venegas, S.A., 1997. A manual for EOF and SVD analyses of climatic data. CCGCR Report No. 97-1, McGill University, Montréal, 52 pp.

Boyaj, A. and Vijayaraghavan, S., 2025. Quantifying long-term variability and extremes in Southeast Asia's rainfall: a 40-year observational study (1980–2019). Theoretical and Applied Climatology, 156(7), p.416.

Cai, W., Yang, K., Wu, L., Huang, G., Santoso, A., Ng, B., Wang, G. and Yamagata, T., 2021. Opposite response of strong and moderate positive Indian Ocean Dipole to global warming. Nature Climate Change, 11(1), pp.27-32.

Cai, W., Zheng, X.T., Weller, E., Collins, M., Cowan, T., Lengaigne, M., Yu, W. and Yamagata, T., 2013. Projected response of the Indian Ocean Dipole to greenhouse warming. Nature Geoscience, 6(12), pp.999-1007.

Chan, J.C. and Li, C., 2004. The east Asia winter monsoon. In East Asian Monsoon (pp.54-106.

Chang, C.P., Wang, Z., McBride, J. and Liu, C.H., 2005. Annual cycle of Southeast Asia-Maritime Continent rainfall and the asymmetric monsoon transition. Journal of Climate, 18(2), pp.287-301.

Chemke, R. and Polvani, L.M., 2021. Elucidating the mechanisms responsible for Hadley cell weakening under 4× CO2 forcing. Geophysical Research Letters, 48(3), p.e2020GL090348.

Ciesielski, P.E. and Johnson, R.H., 2022. Extended analysis of the effects of the Sumatra topography on downstream low-level vortex development over the Indian Ocean. arXiv preprint arXiv:2210.14370.

Deser, C., Alexander, M.A., Xie, S.-P. and Phillips, A.S., 2010. Sea surface temperature variability: Patterns and mechanisms. Annual Review of Marine Science, 2, pp.115–143.

Deser, C., Phillips, A., Bourdette, V. and Teng, H., 2012. Uncertainty in climate change projections: the role of internal variability. Climate Dynamics, 38(3), pp.527-546.

Du, Y., Xie, S.P., Huang, G. and Hu, K., 2009. Role of air–sea interaction in the long persistence of El Niño–induced north Indian Ocean warming. Journal of Climate, 22(8), pp.2023-2038.

Endo, N., Matsumoto, J. and Lwin, T., 2009. Trends in precipitation extremes over Southeast Asia. Sola, 5, pp.168-171.

Feng, X., Hodges, K.I., Hoang, L., Pura, A.G., Yang, G.Y., Luu, H., David, S.J., Duran, G.A.M. and Guo, Y.P., 2022. A new approach to skillful seasonal prediction of Southeast Asia tropical cyclone occurrence. Journal of Geophysical Research: Atmospheres, 127(12), p.e2022JD036439.

Ferrett, S., Methven, J., Woolnough, S.J., Yang, G.Y., Holloway, C.E. and Wolf, G., 2023. Hybrid dynamical–statistical forecasts of the risk of rainfall in Southeast Asia dependent on equatorial waves. Monthly Weather Review, 151(8), pp.2139-2152.

Geen, R., Bordoni, S., Battisti, D.S. and Hui, K., 2020. Monsoons, ITCZs, and the concept of the global monsoon. Reviews of Geophysics, 58(4), p.e2020RG000700.

Gupta, H. and Sil, S., 2024. Assessment of GHRSST and OISST datasets in identification of marine heat-waves and heat-spikes. IEEE Geoscience and Remote Sensing Letters, 21, pp.1-5.

Ha, K.J., Heo, K.Y., Lee, S.S., Yun, K.S. and Jhun, J.G., 2012. Variability in the East Asian monsoon: A review. Meteorological Applications, 19(2), pp.200-215.

Hawkins, E. and Sutton, R., 2009. The potential to narrow uncertainty in regional climate predictions. Bulletin of the American Meteorological Society, 90(8), pp.1095-1108.

Hersbach, H., Bell, B., Berrisford, P., Hirahara, S., Horányi, A., Muñoz-Sabater, J., Nicolas, J., Peubey, C., Radu, R., Schepers, D. and Simmons, A., 2020. The ERA5 global reanalysis. Quarterly Journal of the Royal Meteorological Society, 146(730), pp.1999-2049.

Huang, B., L'Heureux, M., Lawrimore, J., Liu, C., Zhang, H.M., Banzon, V., Hu, Z.Z. and Kumar, A., 2013. Why did large differences arise in the sea surface temperature datasets across the tropical Pacific during 2012? Journal of Atmospheric and Oceanic Technology, 30(12), pp.2944-2953.

Huang, B., Liu, C., Banzon, V., Freeman, E., Graham, G., Hankins, B., Smith, T. and Zhang, H.M., 2021. Improvements of the daily optimum interpolation sea surface temperature (DOISST) version 2.1. Journal of Climate, 34(8), pp.2923-2939.

Hung, N.T., Boyaj, A., Raghavan, S.V., Son, N.N. and Ona, B.J., 2026. Performance Evaluation of the MPAS Model in Simulating Southeast Asian Rainfall Characteristics. International Journal of Climatology, p.e70343.

Juneng, L. and Tangang, F.T., 2005. Evolution of ENSO-related rainfall anomalies in Southeast Asia region and its relationship with atmosphere–ocean variations in Indo-Pacific sector. Climate Dynamics, 25(4), pp.337-350.

Kajikawa, Y., Wang, B. and Yang, J., 2010. A multi-time scale Australian monsoon index. International Journal of Climatology, 30(8), pp.1114–1120.

Kamae, Y., Watanabe, M., Kimoto, M. and Shiogama, H., 2014. Summertime land–sea thermal contrast and atmospheric circulation over East Asia in a warming climate Part I: Past changes and future projections. Climate Dynamics, 43(9), pp.2553-2568.

Kitoh, A., 2017. The Asian monsoon and its future change in climate models: A review. Journal of the Meteorological Society of Japan. Ser. II, 95(1), pp.7-33.

Klein, S.A., Soden, B.J. and Lau, N.C., 1999. Remote sea surface temperature variations during ENSO: Evidence for a tropical atmospheric bridge. Journal of Climate, 12(4), pp.917-932.

Kosaka, Y. and Xie, S.P., 2013. Recent global-warming hiatus tied to equatorial Pacific surface cooling. Nature, 501(7467), pp.403-407.

Kumari, P., Preethi, B. and Mujumdar, M., 2025. Climatological characteristics of ITCZ over the South Asian monsoon domain: Using multivariate probabilistic approach. Atmospheric Research, p.108709.

Lavers, D.A., Simmons, A., Vamborg, F. and Rodwell, M.J., 2022. An evaluation of ERA5 precipitation for climate monitoring. Quarterly Journal of the Royal Meteorological Society, 148(748), pp.3152-3165.

Li, X., Li, Q., Ding, Y., Yang, S., Dong, L., Yu, J., Shen, X., Wu, Q. and Sun, X., 2023. Possible influence of the interdecadal variation of the extratropical southern Indian Ocean SST on East Asian summer monsoon precipitation. Atmospheric Research, 288, p.106721.

Liu, L., Xu, Z.X. and Huang, J.X., 2012. Spatio-temporal variation and abrupt changes for major climate variables in the Taihu Basin, China. Stochastic Environmental Research and Risk Assessment, 26(6), pp.777-791.

Mallakpour, I. and Villarini, G., 2016. A simulation study to examine the sensitivity of the Pettitt test to detect abrupt changes in mean. Hydrological Sciences Journal, 61(2), pp.245-254.

Meehl, G.A., Teng, H. and Arblaster, J.M., 2014. Climate model simulations of the observed early-2000s hiatus of global warming. Nature Climate Change, 4(10), pp.898-902.

North, G.R., Bell, T.L., Cahalan, R.F. and Moeng, F.J., 1982. Sampling errors in the estimation of empirical orthogonal functions. Monthly Weather Review, 110(7), pp.699–706.

Pettitt, A.N., 1979. A non-parametric approach to the change-point problem. Journal of the Royal Statistical Society: Series C (Applied Statistics), 28(2), pp.126-135.

Purwar, S., Rakesh, V., Bankar, A. and Mohapatra, G.N., 2023. Relationship of height and intensity of low-level jet stream with Indian summer monsoon rainfall. Theoretical and Applied Climatology, 151(1), pp.785-799.

Qian, J.H., Robertson, A.W. and Moron, V., 2010. Interactions among ENSO, the monsoon, and diurnal cycle in rainfall variability over Java, Indonesia. Journal of the Atmospheric Sciences, 67(11), pp.3509-3524.

Rasmusson, E.M. and Carpenter, T.H., 1982. Variations in tropical sea surface temperature and surface wind fields associated with the Southern Oscillation/El Niño. Monthly Weather Review, 110(5), pp.354-384.

Saji, N.H., Goswami, B.N., Vinayachandran, P.N. and Yamagata, T., 1999. A dipole mode in the tropical Indian Ocean. Nature, 401(6751), pp.360–363.

Sharmar, V. and Markina, M., 2020. Validation of global wind wave hindcasts using ERA5, MERRA2, ERA-Interim and CFSRv2 reanalyses. IOP Conference Series: Earth and Environmental Science, 606, p.012056.

Shaw, T.A. and Voigt, A., 2015. Tug of war on summertime circulation between radiative forcing and sea surface warming. Nature Geoscience, 8(7), pp.560-566.

Song, F., Zhou, T. and Qian, Y., 2014. Responses of East Asian summer monsoon to natural and anthropogenic forcings in the 17 latest CMIP5 models. Geophysical Research Letters, 41(2), pp.596–603.

Swetha, S., Ramesh, K.V. and Rakesh, V., 2025. Influence of large-scale climate modes (ENSO, IOD and PJ) on marine heatwave characteristics in the Indian ocean region. Theoretical and Applied Climatology, 156(6), p.343.

Tangang, F.T., Juneng, L., Salimun, E., Vinayachandran, P.N., Seng, Y.K., Reason, C.J.C., Behera, S.K. and Yasunari, T., 2008. On the roles of the northeast cold surge, the Borneo vortex,

the Madden-Julian Oscillation, and the Indian Ocean Dipole during the extreme 2006/2007 flood in southern Peninsular Malaysia. Geophysical Research Letters, 35(14).

Tarek, M., Brissette, F.P. and Arsenault, R., 2020. Evaluation of the ERA5 reanalysis as a potential reference dataset for hydrological modelling over North America. Hydrology and Earth System Sciences, 24(5), pp.2527-2544.

Thapliyal, R., 2023. The monsoon low-level jet: climatology and impact on monsoon rainfall over the west coast and central peninsular India. Journal of Meteorological Research, 37(1), pp.112-125.

Tokinaga, H., Xie, S.P., Deser, C., Kosaka, Y. and Okumura, Y.M., 2012. Slowdown of the Walker circulation driven by tropical Indo-Pacific warming. Nature, 491(7424), pp.439-443.

Trenberth, K.E., Fasullo, J.T., Branstator, G. and Phillips, A.S., 2014. Seasonal aspects of the recent pause in surface warming. Nature Climate Change, 4(10), pp.911-916.

Trenberth, K.E., Stepaniak, D.P. and Caron, J.M., 2000. The global monsoon as seen through the divergent atmospheric circulation. Journal of Climate, 13(22), pp.3969-3993.

Vecchi, G.A. and Soden, B.J., 2007. Global warming and the weakening of the tropical circulation. Journal of Climate, 20(17), pp.4316-4340.

Villafuerte, M.Q. and Matsumoto, J., 2015. Significant influences of global mean temperature and ENSO on extreme rainfall in Southeast Asia. Journal of Climate, 28(5), pp.1905-1919.

Villarini, G., Serinaldi, F., Smith, J.A. and Krajewski, W.F., 2009. On the stationarity of annual flood peaks in the continental United States during the 20th century. Water Resources Research, 45(8).

Wang, B. and Fan, Z., 1999. Choice of South Asian summer monsoon indices. Bulletin of the American Meteorological Society, 80(4), pp.629-638.

Wang, B., 2006. The Asian monsoon. Springer Science and Business Media.

Wang, B., Liu, J., Kim, H.J., Webster, P.J. and Yim, S.Y., 2012. Recent change of the global monsoon precipitation (1979–2008). Climate Dynamics, 39(5), pp.1123-1135.

Wang, B., Wu, R. and Lau, K.M., 2001. Interannual variability of the Asian summer monsoon: Contrasts between the Indian and the western North Pacific–East Asian monsoons. Journal of Climate, 14(20), pp.4073-4090.

Webster, P.J., Moore, A.M., Loschnigg, J.P. and Leben, R.R., 1999. Coupled ocean–atmosphere dynamics in the Indian Ocean during 1997–98. Nature, 401(6751), pp.356–360.

Wei, Y., Peng, K., Ma, Y., Sun, Y., Zhao, D., Ren, X., Yang, S., Ahmad, M., Pan, X., Wang, Z. and Xin, J., 2024. Validation of ERA5 boundary layer meteorological variables by remote-sensing measurements in the Southeast China mountains. Remote Sensing, 16(3), p.548.

Wilks, D.S., 2011. Statistical Methods in the Atmospheric Sciences, 3rd edn. International Geophysics Series, Vol. 100, Academic Press, 676 pp.

Xie, S.P., Chang, C.H., Xie, Q. and Wang, D., 2007. Intraseasonal variability in the summer South China Sea: Wind jet, cold filament, and recirculations. Journal of Geophysical Research: Oceans, 112(C10).

Xie, Y., Wang, J., Wan, X. and Lyu, Y., 2025. Assessing the monthly performance of daily precipitation products over Southeast Asia using the gauge-based analysis. Plos one, 20(3), p.e0319477.

Xu, L., Zhang, T., Wang, A., Yu, W. and Yang, S., 2022. Variations of summer extreme and total precipitation over Southeast Asia and associated atmospheric and oceanic features. Journal of Climate, 35(19), pp.6395-6409.

772 Zhang, X., Alexander, L., Hegerl, G.C., Jones, P., Tank, A.K., Peterson, T.C., Trewin, B. and
773 Zwiers, F.W., 2011. Indices for monitoring changes in extremes based on daily temperature and
774 precipitation data. Wiley Interdisciplinary Reviews: Climate Change, 2(6), pp.851-870.

Figures

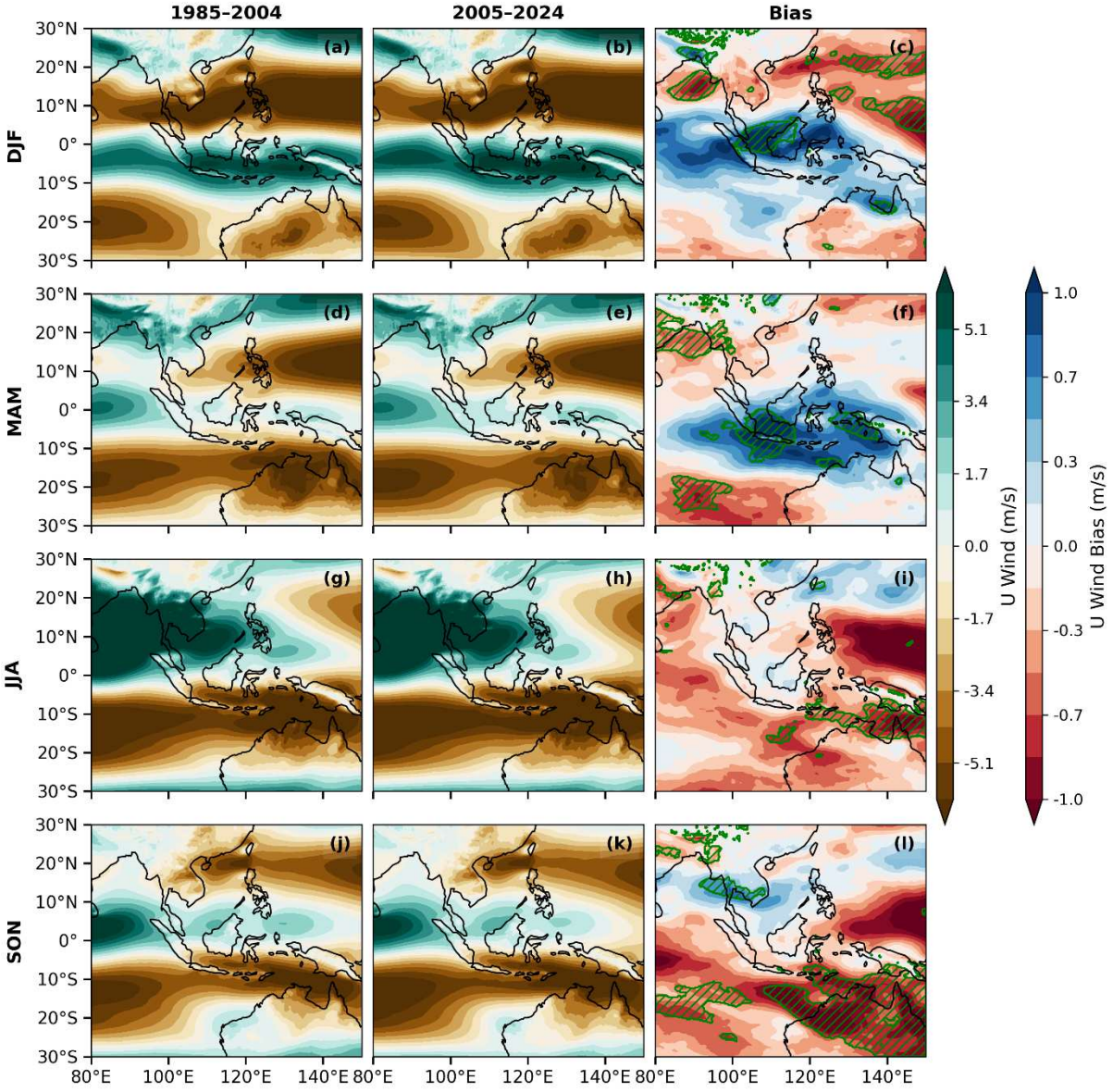


Figure 1. Spatial climatological patterns of seasonal zonal wind (U; m s^{-1}) at 850 hPa over SEA for the past (1985-2004; first column) and recent (2005-2024; second column) climate periods, and their biases (recent minus past; third column). The rows (from top to bottom) represent the seasons DJF, MAM, JJA, and SON. Positive values indicate westerlies (eastward flow), while negative values indicate easterlies (westward flow). The green hatching (third column) represents the statistically significant change area at a 95% confidence level.

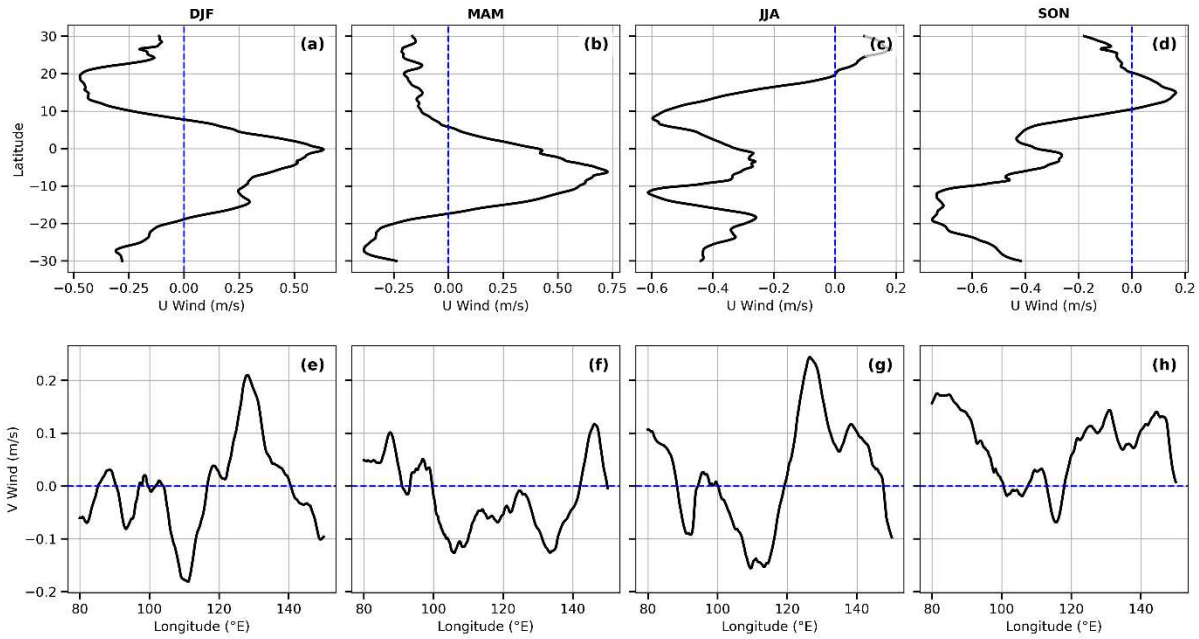


Figure 2. Seasonal differences (2005–2024 minus 1985–2004) in the 850 hPa zonal (U) and meridional (V) wind components over Southeast Asia (SEA). The top row shows the longitudinally averaged zonal wind (80°–150°E) as a function of latitude, while the bottom row shows the latitudinally averaged meridional wind (30°S–30°N) as a function of longitude. Columns correspond to the four seasons: DJF, MAM, JJA, and SON.

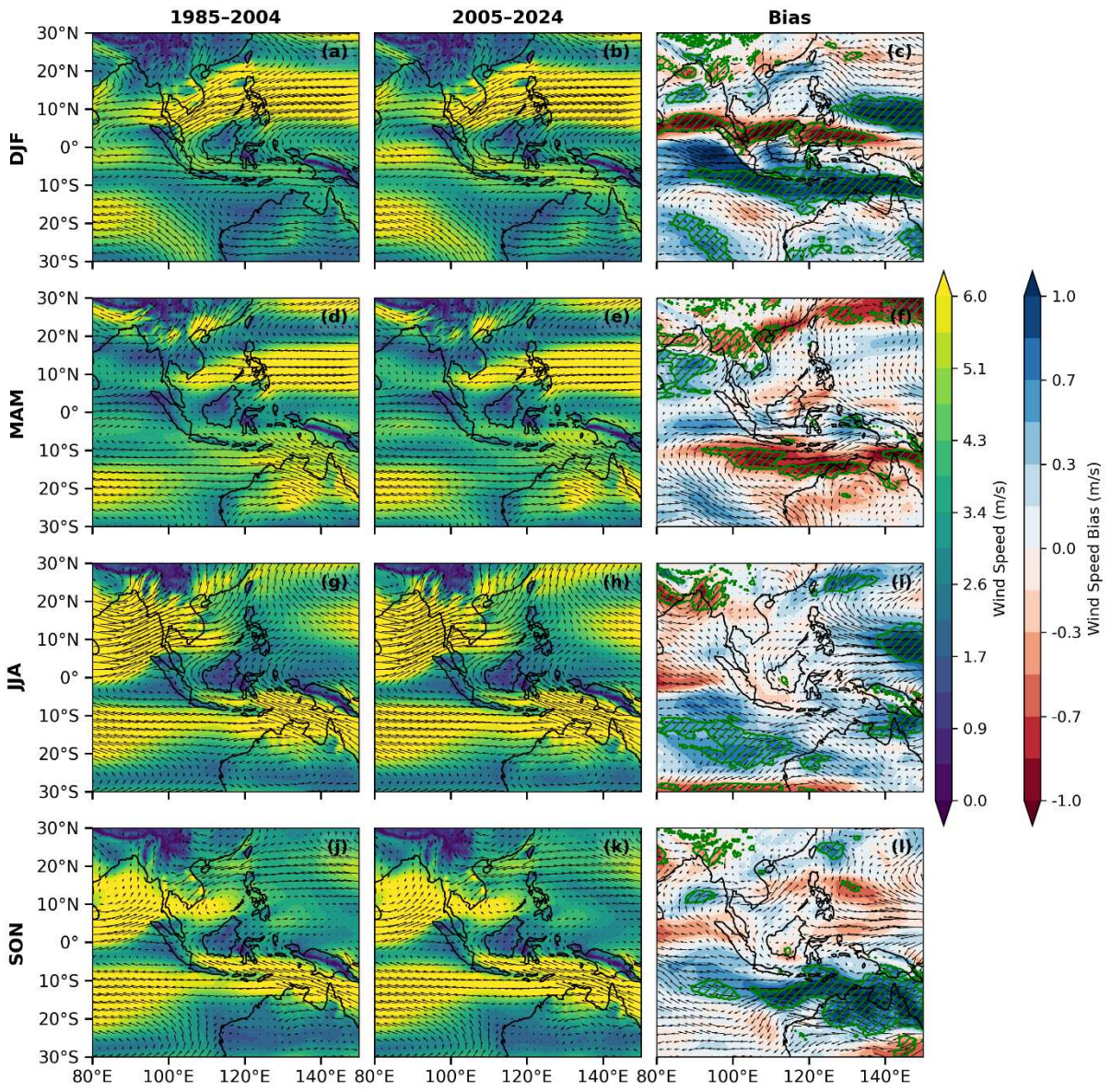


Figure 3. Spatial climatological patterns of seasonal wind speed (m s^{-1}) at 850 hPa (shaded) and vectors (arrows) over SEA for the past (first column) and recent (second column) climate periods, and their differences (recent minus past; third column). The rows (from top to bottom) represent the seasons DJF, MAM, JJA, and SON. The green hatching (third column) represents the statistically significant change area at a 95% confidence level.

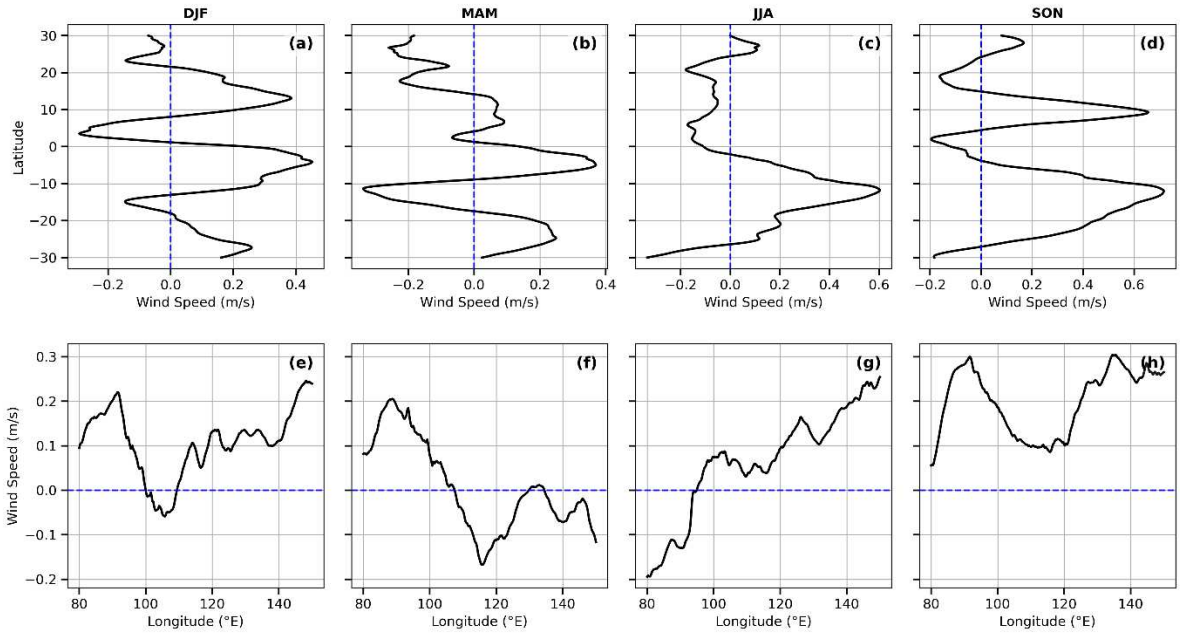


Figure 4. Differences in wind speed (m s^{-1}) between the recent (2005–2024) and past (1985–2004) climate periods (recent minus past) over SEA. The top row shows the meridional structure of the wind speed, averaged longitudinally over 80°–150°E, while the bottom row shows the zonal structure of the wind speed, averaged latitudinally over 30°S–30°N. Columns correspond to the four seasons: DJF, MAM, JJA, and SON. Few grid points show statistically significant trends in the two 20-year sub-periods (second and third columns).

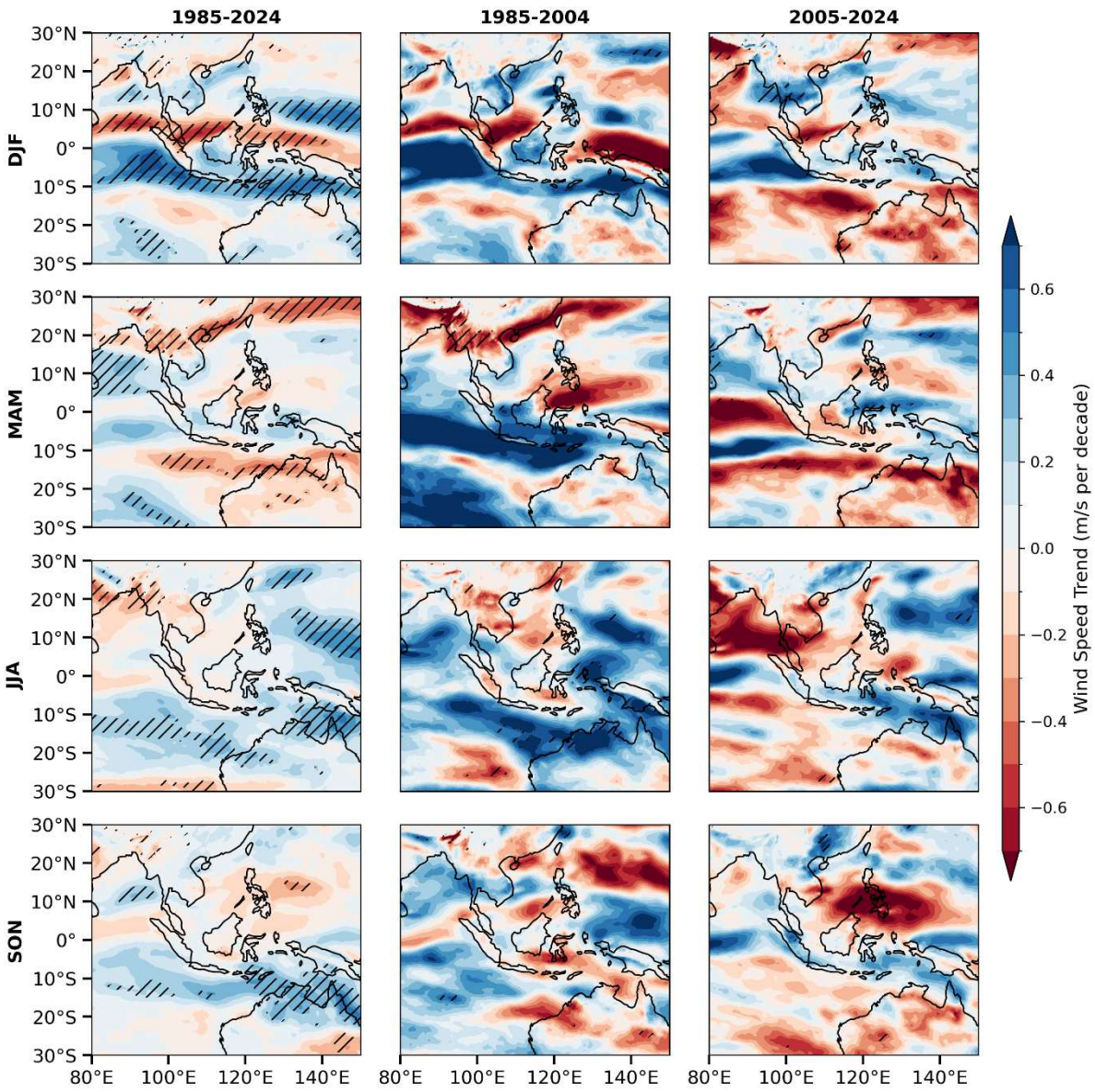


Figure 5. Spatial distribution of temporal trends in the seasonal wind speed (m s^{-1} $decade^{-1}$) over SEA. Columns (left to right) represent the periods 1985–2024, 1985–2004, and 2005–2024. Rows (top to bottom) correspond to DJF, MAM, JJA, and SON. Blue (red) shading indicates positive (negative) trends, with black hatching denoting statistically significant trend area at the 95% confidence level.

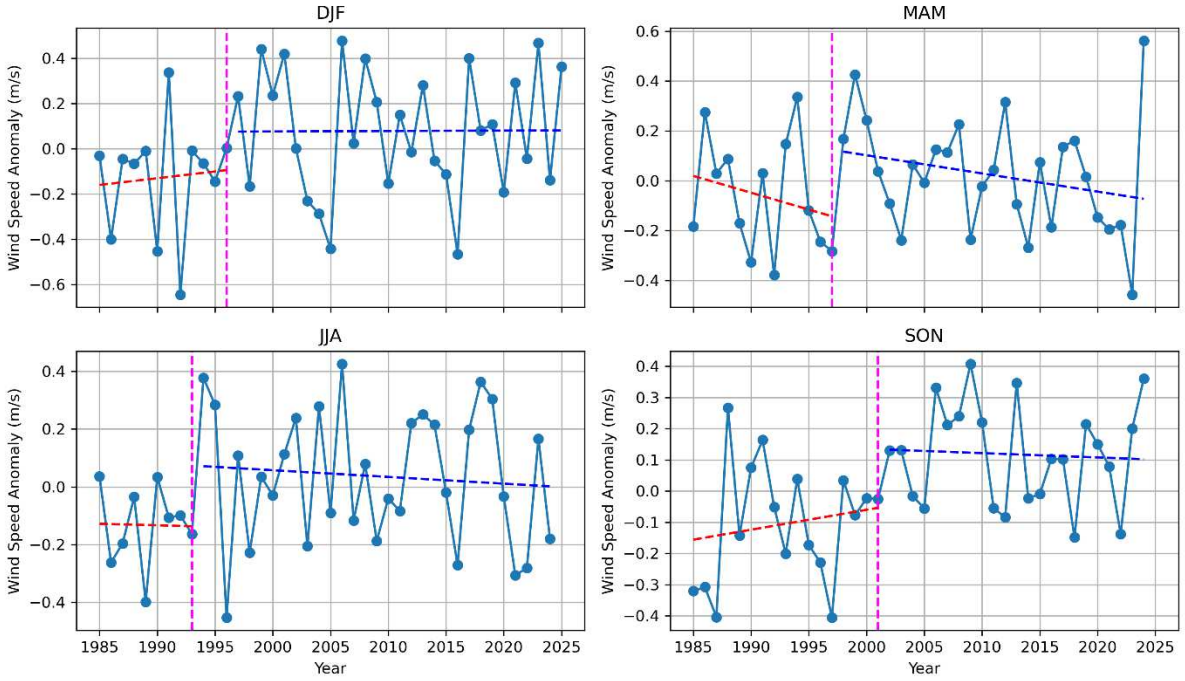


Figure 6. Time series of area-averaged seasonal wind speed anomalies (m s^{-1}) at 850 hPa over SEA for DJF, MAM, JJA and SON. The magenta dashed vertical line indicates the respective change point estimated by the Pettitt test (1996 for DJF, 1997 for MAM, 1993 for JJA, and 2001 for SON); only the SON change point is statistically significant at the 95% confidence level. Red and blue dashed lines show linear trends before and after the respective change point.

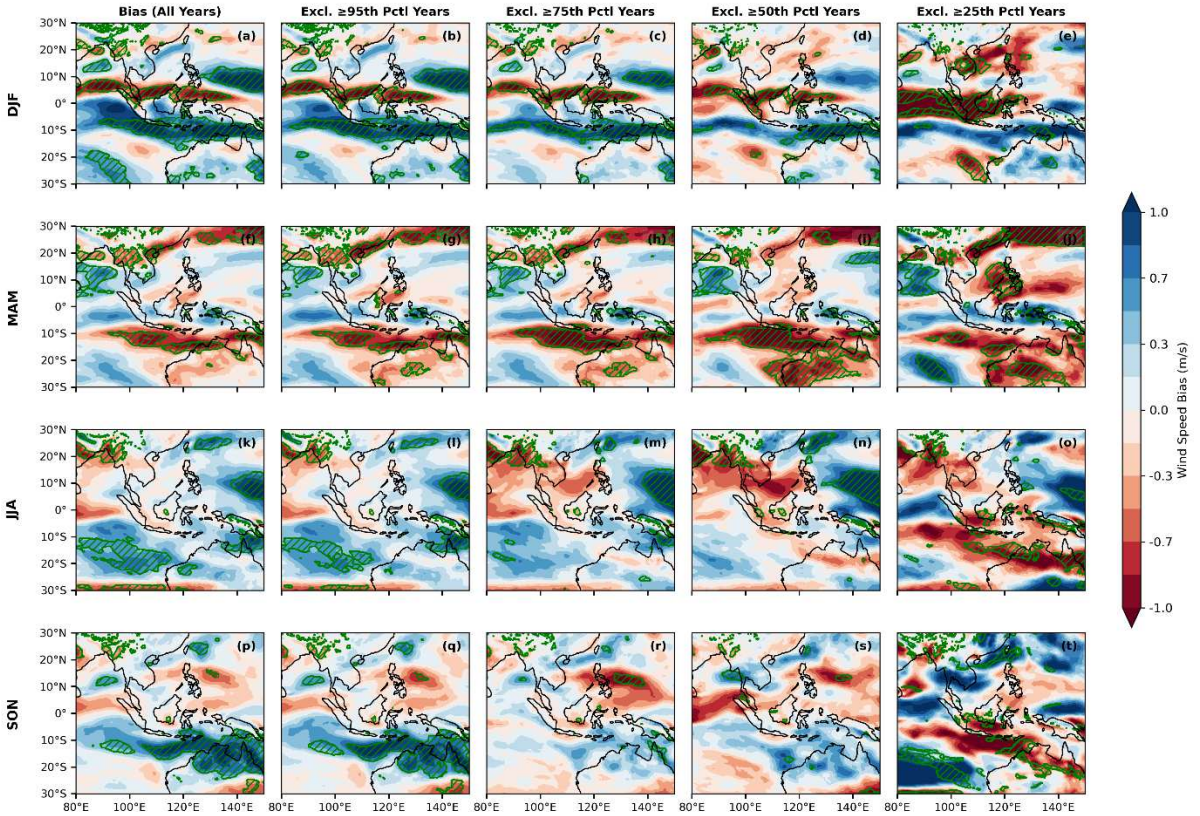


Figure 7. Spatial distribution of seasonal mean wind speed differences (m s^{-1}) between the recent and past climate periods, shown with and without the removal of recent-period years. The first column includes all years, while the second to fifth columns cumulatively exclude the recent-period years at or above the 95th, 75th, 50th, and 25th percentiles of area-averaged seasonal wind speed, respectively. Rows (top to bottom) correspond to DJF, MAM, JJA, and SON. Areas with statistically significant changes at the 95% confidence level are indicated by green hatching.

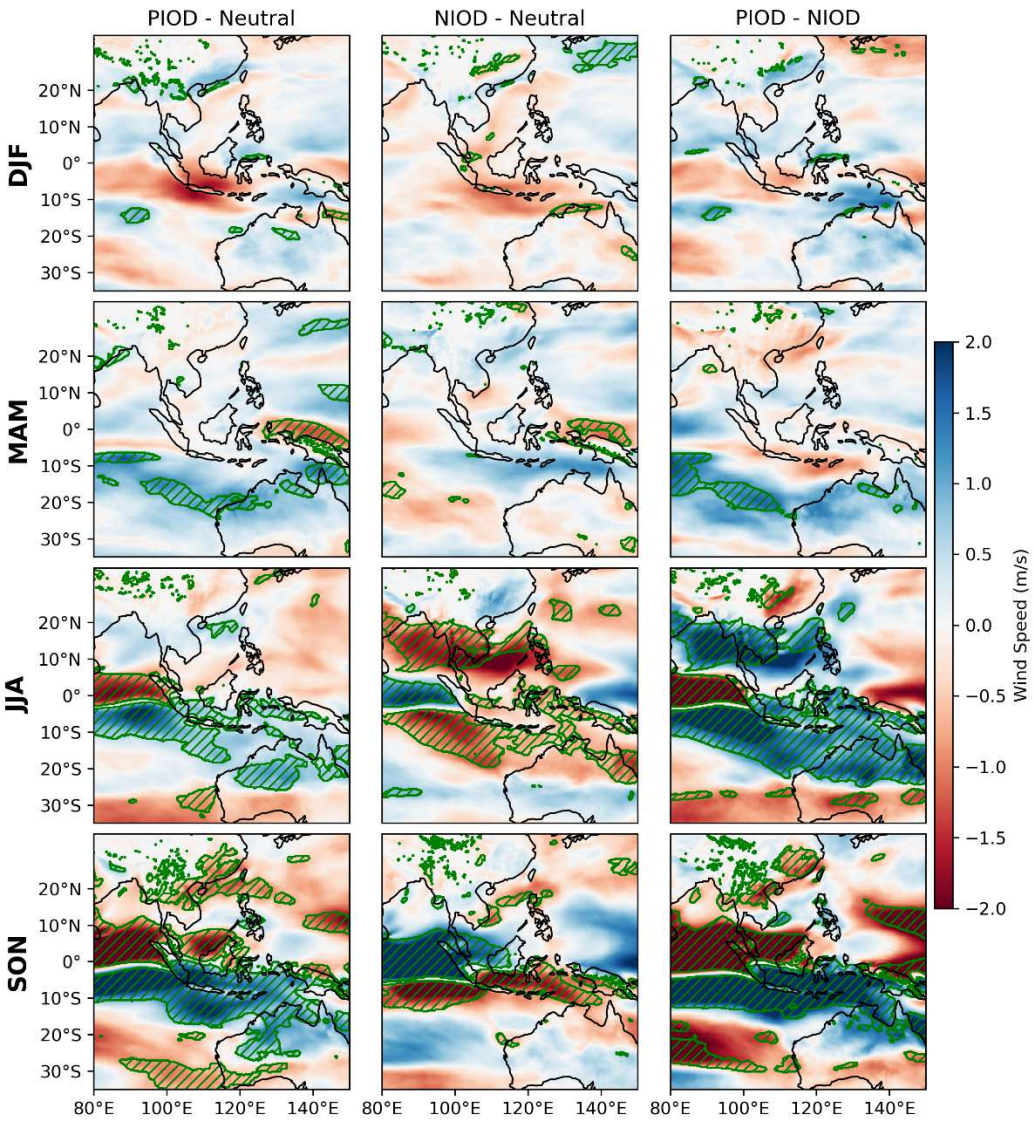


Figure 8. Spatial distribution of composite wind speed differences between strong positive IOD (PIOD) years and neutral years (first column), strong negative IOD (NIOD) years and neutral years (second column), and strong positive IOD and negative IOD years (third column). Rows (from top to bottom) correspond to the DJF, MAM, JJA, and SON seasons. Green hatching indicates regions where the differences are statistically significant at the 95% confidence level.

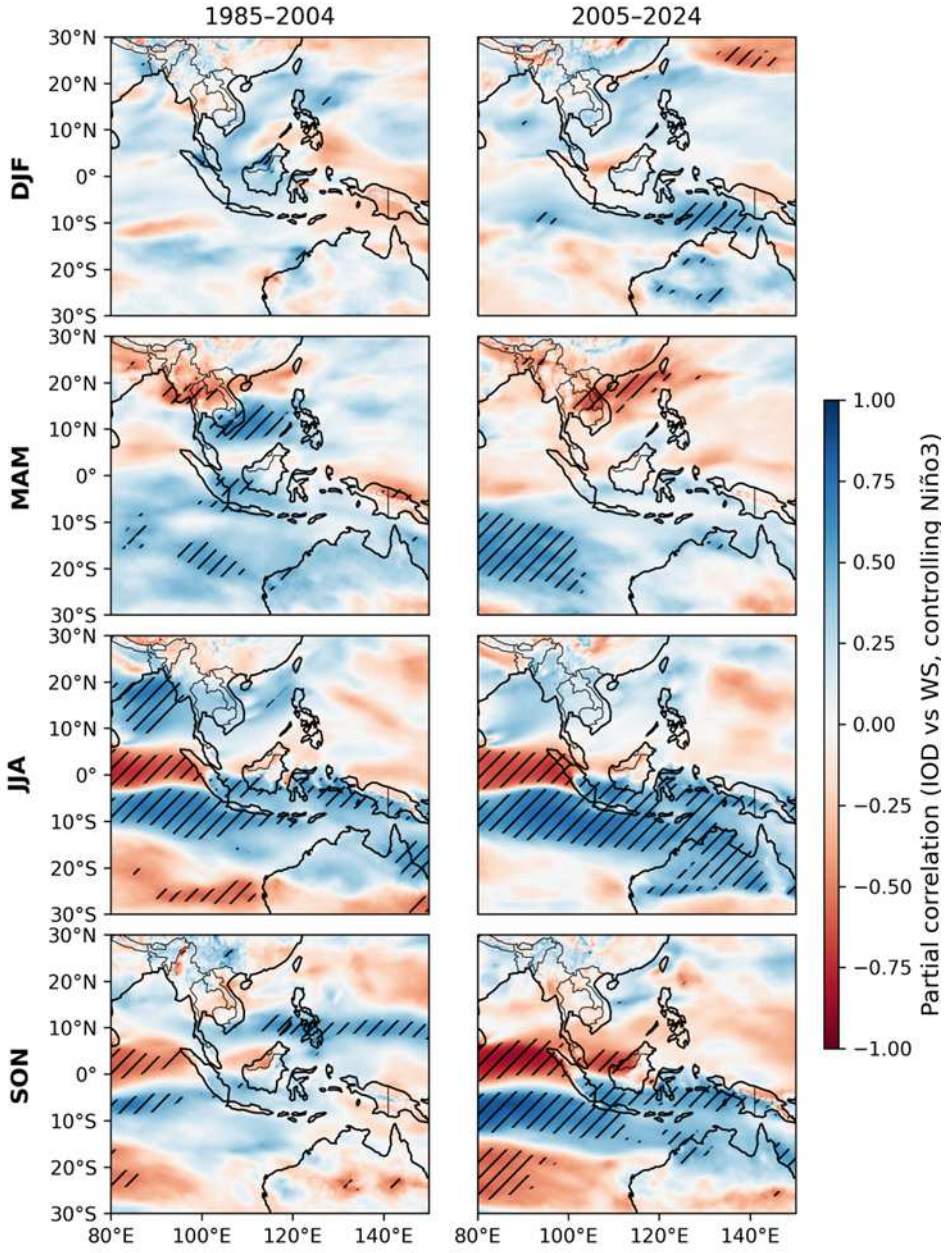


Figure 9. Spatial distribution of the partial correlation between IOD and wind speed anomalies during the past (left column) and recent (right column) climate periods. Rows (from top to bottom) represent DJF, MAM, JJA, and SON. Areas with black hatching indicate regions that are statistically significant at the 95% confidence level.

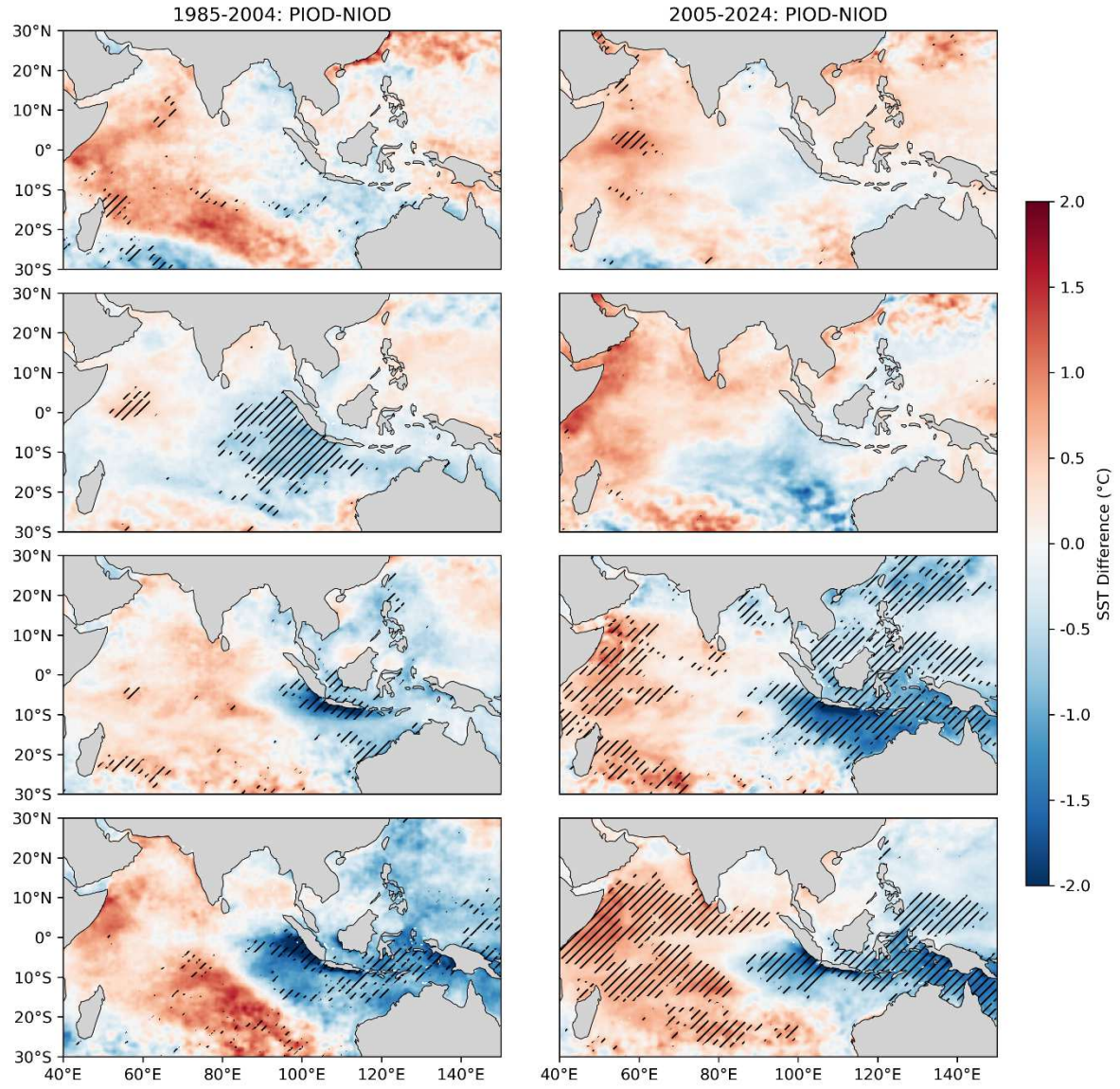


Figure 10. Spatial distribution of composite sea surface temperature differences between strong positive IOD (PIOD) and negative IOD (NIOD) years during the past (first column) and recent (second column) climate periods. Rows (from top to bottom) correspond to the DJF, MAM, JJA, and SON seasons. Black hatching indicates regions where the differences are statistically significant at the 95% confidence level.

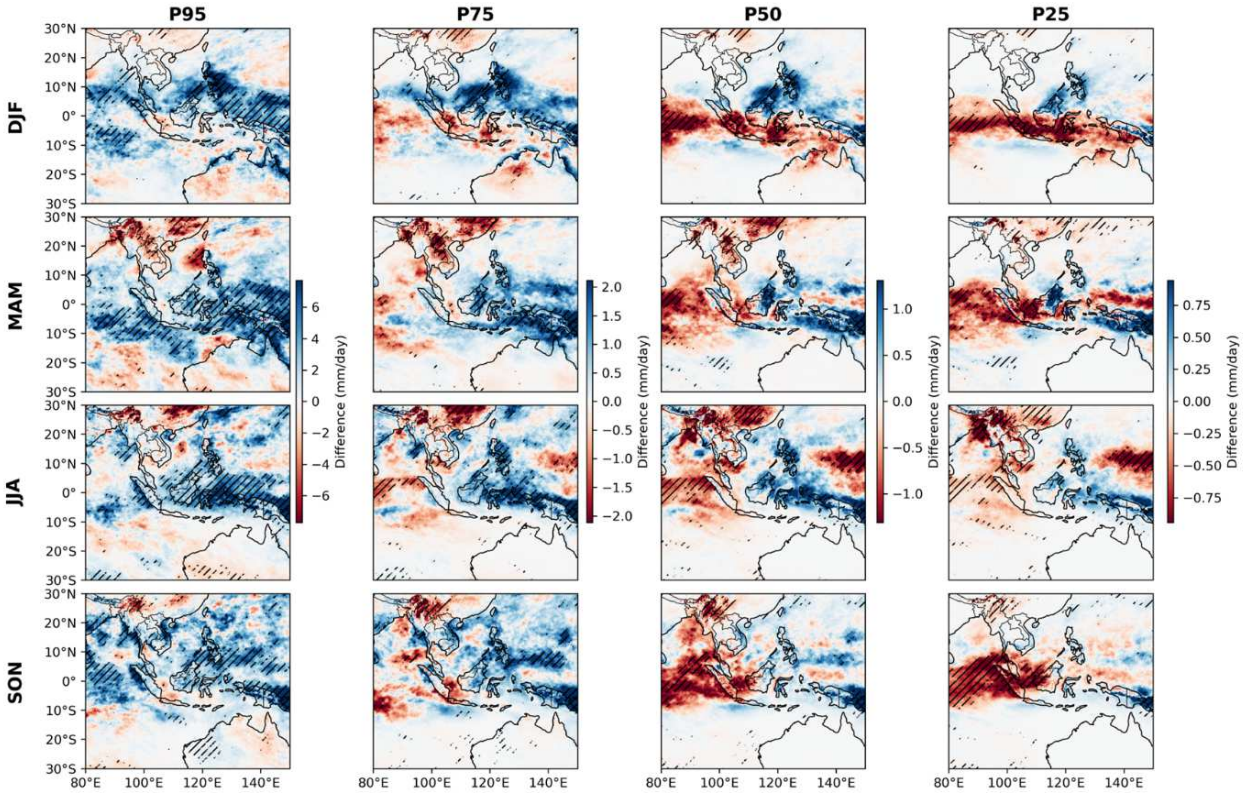


Figure 11. Spatial distribution of seasonal rainfall magnitude differences (mm/day) between the recent (2005–2024) and past (1985–2004) climate periods over SEA for the 95th (first column), 75th (second column), 50th (third column), and 25th (fourth column) percentiles. The rows (from top to bottom) represent the seasons DJF, MAM, JJA, and SON. Black hatching indicates areas where the changes are statistically significant at the 95% confidence level. The blue and red color shading represent the increase and decrease in rainfall magnitude, respectively.

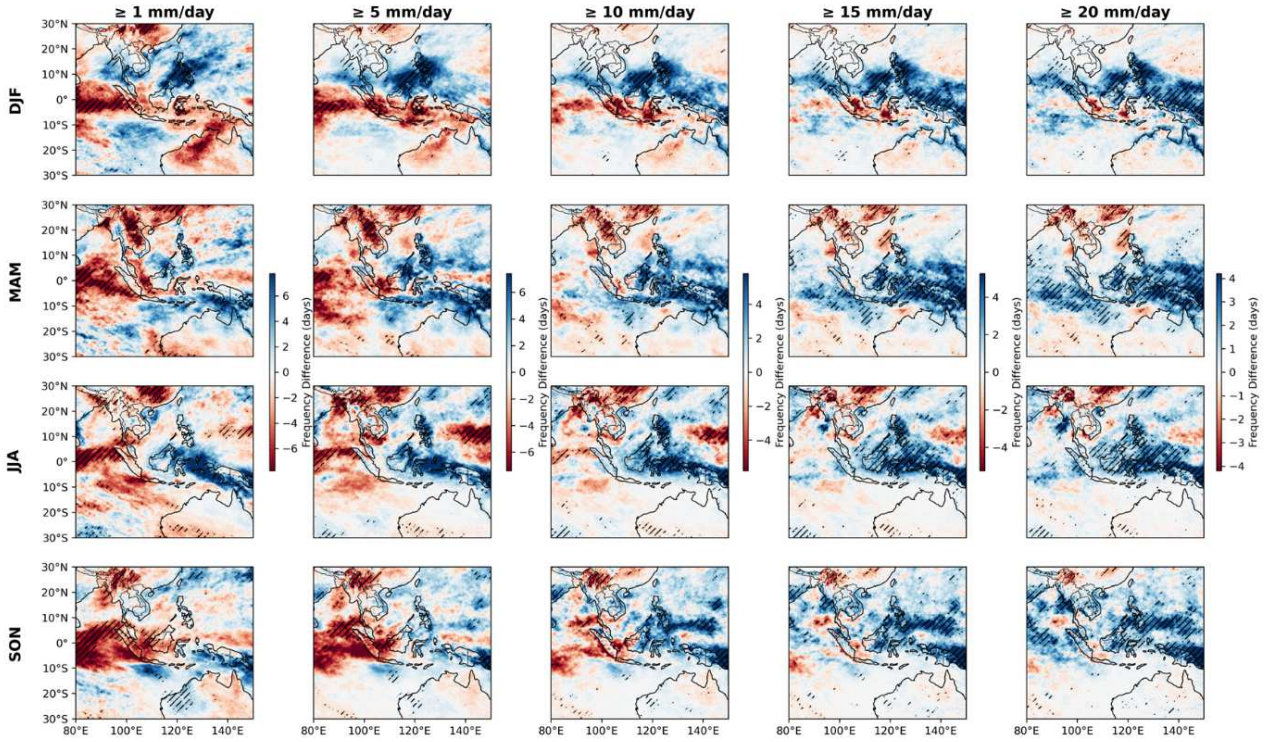


Figure 12. Spatial distribution of seasonal rainfall frequency differences (days) between the recent (2005–2024) and past (1985–2004) climate periods for the 1 mm (first column), 5 mm (second column), 10 mm (third column), 15 mm (fourth column), and 20 mm (fifth column) rainfall magnitude frequency. The rows (from top to bottom) represent the seasons DJF, MAM, JJA, and SON. Black hatching indicates areas where the changes are statistically significant at the 95% confidence level. The blue and red color shading represent the increase and decrease in rainfall frequency, respectively.

Supplementary Files

This is a list of supplementary files associated with this preprint. Click to download.

- SEAtradewindssupplymaterial16Oct2026.docx